Complex potential surface for the $^2B_1$ metastable state of the water anion

Daniel J. Haxton,[1,2,*] Zhiyong Zhang,[2,†] C. William McCurdy,[2,3,1,‡] and Thomas N. Rescigno[2,§]

[1] *Department of Chemistry, University of California, Berkeley, California 94720*
[2] *Lawrence Berkeley National Laboratory, Computing Sciences, Berkeley, California 94720*
[3] *Department of Applied Science, University of California, Davis, California 95616*

The potential energy surface corresponding the complex resonance energy of the $^2B_1$ Feshbach resonance state of the water anion is constructed in its full dimensionality. Complex Kohn variational scattering calculations are used to compute the resonance width, while large-scale Configuration Interaction calculations are used to compute the resonance energy. Near the equilibrium geometry, an accompanying ground state potential surface is constructed from Configuration Interaction calculations that treat correlation at a level similar to that used in the calculations on the anion.

I. INTRODUCTION

At kinetic energies of less than about 15 eV, electron impacts with water molecules are capable of leading to the formation of resonance states that are dissociative, or to the excitation of low-lying singlet and triplet electronic states, many of which are also dissociative. Thus, collisions of low-energy electrons with water can initiate chemical reactions involving both radical and ionic fragments of the water molecule. While such processes are certainly interesting on a purely theoretical level, they gain additional relevance through their suspected complicity in mechanisms of genome damage in living organisms. In the presence of ionizing radiation in the condensed phase, a shower of low-energy secondary electrons results from essentially all primary ionization events. Therefore dissociative attachment and dissociative excitation of water are candidates to play key roles in the mechanism of radiation damage to biological systems.

In this paper we begin the investigation of dissociative attachment (DA) through the lowest energy Feshbach resonance state of the water anion, which in the C_{2v} symmetry of the equilibrium geometry of the water molecule has $^2B_1$ symmetry. Here we address the problem of constructing a complete potential energy surface of this metastable state which determines the motion of the nuclei during the dissociative attachment process. In the following article, we will investigate the quantum dynamics of dissociative attachment on this surface. That study will make use of the local complex potential model for the nuclear dynamics, in which the nuclei move on the complex potential surface

$$V = E_R - i\Gamma/2 \quad , \tag{1}$$

where E_R and $-\Gamma/2$ are the real and imaginary parts, respectively, of the well-defined complex resonance energy of the $^2B_1$ state.

Not surprisingly, negative ion formation has been the subject of intense experimental and theoretical investigation, starting as early as 1930 [1]. Early experiments on negative ion formation by electron impact focused mainly on the identification of the negative ion species formed, the measurement of the total cross sections, and the energy locations of the structures in the resonance process [2]. Buchel'nikova [3] and Schultz [4] established that the main products of dissociative electron attachment in water are H^- and O^- , with the production of O^- being much smaller than that of H^- at lower energies, but with O^- dominating at higher electron-impact energies.

Compton and Christophorou [5] carried out a comprehensive study of negative ion formation in water and measured the total cross sections for negative ion production in H_2O. Three resonance peaks were observed. H^- production was observed at approximately 6.5 eV and 8.6 eV, with the second peak much less intense than the first. O^- was observed in increasing intensities in three peaks at 6.9 eV, 8.9 eV, and 11.4 eV, respectively, the first two appearing at slightly higher energies than the corresponding H^- resonance peaks. Isotopic effects were also measured and discussed in detail in this study. Trends similar to H^-/H_2O and O^-/H_2O were observed for the formation of D^- and O^- from D_2O, although some significant differences in peak heights and widths were observed in the case of the deuterated target.

A series of measurements by Trajmar and Hall [6] and Belic, Laudau, and Hall [7] revealed the energy and angular dependence of H^- production in dissociative electron attachment to H_2O. The angular distributions at the three resonance peaks were judged to be consistent with the assignment of the three resonances as having $^2B_1$, $^2A_1$, and $^2B_2$ symmetries, respectively. These measurements also gave detailed information about the vibrational and rotational state distribution of the OH fragments.

Compared with the large number of experimental measurements, detailed theoretical work on dissociative electron-water collisions has been relatively scarce and there has been no previous *ab initio* work on dissociative electron attachment to water. The paucity of theoreti-

*djhaxton@lbl.gov
†zyzhang@lbl.gov
‡cwmccurdy@lbl.gov
§tnrescigno@lbl.gov

cal work on DA stems from the fact that, in water, DA proceeds, not through tunneling shape resonances, but through Feshbach resonances that involve changes in the electronic structure of the target. Early theoretical work focused on the electronic structure [8] and configuration-interaction [9] calculations on various states of H_2O^- that are possible resonances. These calculations, together with experimental observations, formed the basis of the assignment of the three Feshbach resonances that are responsible for electron-impact dissociation of water in the gas phase. Contemporary theoretical work has included *ab initio* complex Kohn [10] and R-matrix [11] calculations, at the equilibrium nuclear geometry, of the resonances and excitation cross sections into low-lying dissociative electronic states. More recently, Gorfinkiel, Morgan, and Tennyson [12] carried out R-matrix calculations of dissociative excitation of water through four low-lying excited states (the $^{1,3}B_1$ and $^{3,1}A_1$ states). A limited study of the effects of nuclear motion were included in that work by increasing one of the OH bonds while keeping the equilibrium HOH bond angle and the other OH bond length constant. The only theoretical work on the dynamical aspects of dissociative electron attachment to water are earlier classical trajectory analyses based on either repulsive [13] or attractive [14] model resonace surfaces.

This paper describes the construction of the complex potential energy surface of the first dissociative attachment resonance, the $^2B_1$ state near 6.5 eV, in its full dimensionality. A potential energy surface for the neutral molecule is also constructed at a corresponding level of theory. The imaginary part of the potential surface in Eq.(1) is constructed from calculations using the complex Kohn variational method [15, 16], while the real part of the potential surface, E_R in Eq.(1), is constructed from large-scale configuration-interaction (CI) calculations. Within the local complex potential approximation [17–19], the complex anion surface and the ground-state target surface are sufficient to describe the full dynamics of the dissociative attachment process via the $^2B_1$ resonance.

We will refer to several different coordinate systems in this paper. These are illustrated in Fig. 1. The valence-bond coordinate system is comprised of the OH bond lengths, r_1 and r_2, and the H-O-H bond angle, θ. There are also two different Jacobi coordinate systems; one incorporates an OH bond length, r, the distance between that OH center of mass and the other H, denoted R, and the angle between the r and R vectors, called γ, such that $\gamma = 0$ indicates a collinear H-H-O geometry. The other denotes the H-H separation by r, the distance between the O and the H_2 center of mass by R, and the angle between $\vec{r}$ and $\vec{R}$ by γ. Finally, the triangular coordinate system is comprised of the three internuclear separations r_1, r_2, and r_{HH}.

A subsequent paper will present the results of a study of the full quantum dynamics of the dissociative attachment process on this complex potential surface, which has

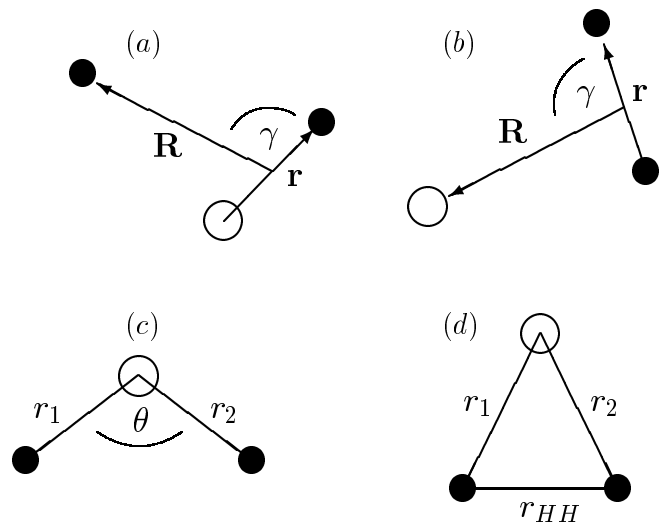

FIG. 1: Coordinate systems to which we refer in this paper. (a) Jacobi ($r = r_{OH}$); (b) Jacobi ($r = r_{HH}$); (c) valence-bond; (d) triangular.

been carried out using a time-dependent version of the local complex potential approximation for nuclear motion of the anion. That paper will describe the use of the Multiconfiguration Time-Dependent Hartree method [20–22] for nuclear dynamics to compute cross sections and vibrational and rotational state distributions of the products.

II. ELECTRONIC STRUCTURE AND ELECTRONIC STATES OF H_2O

Near equilibrium geometry ($r_1 = 1.81$ bohr, $r_2 = 1.81$ bohr, $\theta = 104.5°$), the ground state of H_2O is well described by a self-consistent field (SCF) wave function. The SCF orbitals, in order of increasing energy, are labeled $\{1a_1, 2a_1, 1b_2, 3a_1, 1b_1\}$ in C_{2v} symmetry or $\{1a', 2a', 3a', 4a', 1a''\}$ in C_s symmetry. The $1b_2$ and $3a_1$ orbitals are the main bonding orbitals, while the $1b_1$ orbital is nonbonding and contains the oxygen lone-pair electrons, perpendicular to the molecular plane. Important unoccupied orbitals include the $4a_1$ ($5a''$) orbital, which is the antibonding counterpart to the $3a_1$ orbital, and the $2b_2$ ($6a''$) orbital.

There are six low-lying dissociative electronic states of water -$^{1,3}B_1$, $^{1,3}A_1$, and $^{1,3}B_2$ - which, near equilibrium geometry, are well described by promoting an occupied $1b_1, 3a_1$, or $1b_2$ electron into the anti-bonding $4a_1$ orbital. These states are the parents of three doubly excited anion states with configurations $1b_1 4a_1^2$, $3a_1 4a_1^2$, and $1b_2 4a_1^2$, corresponding to the three main dissociative attachment peaks. In addition, there are also $^{3,1}A_2$ excited states in this energy range, of predominantly Rydberg character, obtained by promoting a $1b_1$ electron into the unoccupied $2b_2$ orbital.

The lowest anion state, the $^2B_1$ state, is a Feshbach resonance which becomes an electronically bound state

as the molecule dissociates and the anion energy drops below the neutral ground state energy. In the region of the potential surface where the $^2B_1$ state is a resonance it is quite narrow and nearly parallels the $^3B_1$ state, which is its parent.

In the asymptotic regions, the $^2B_1$ state correlates with either $OH(^2\Pi) + H^-(^1S)$ or $H_2(^1\Sigma) + O^-(^2P)$. The third arrangement channel, $H(^2S) + OH^-(^1\Sigma)$, which has been observed at each of the resonance peaks, is not a direct product of dissociative attachment on the $^2B_1$ resonance surface [23] and is in fact excluded by symmetry as long as coupling to other surfaces is omitted.

III. CALCULATION OF THE RESONANCE ENERGY AND WIDTH

There are two qualitatively different regions of nuclear geometry in a dissociative attachment problem: the region near the equilibrium geometry of the neutral within which the anion is a resonance, and the asymptotic region in which the resonance becomes bound. In the resonance region, the anion has a finite width or inverse lifetime, which can be evaluated either by a direct method using "Fermi's Golden Rule," or by analyzing the results of a fixed-nuclei scattering calculation. In the bound region, the anion can be described using modern electronic structure techniques, e.g., a configuration-interaction calculation.

Because the $^2B_1$resonance is so narrow ($\Gamma \approx 0.006$ eV at the equilibrium geometry of water), one can, in practice, use CI techniques to evaluate the real part of the $^2B_1$ surface at all geometries of interest. This strategy allows one to evaluate the real part of the resonance surface from large-scale CI expansions that would be impossible to use in any practical scattering calculation. Fixed-nuclei scattering calculations, using the complex Kohn variational method, were carried out, but over a more limited set of geometries near the equilibrium position of the target, for the purpose of obtaining the imaginary part of the resonance energies.

In the following sections we will describe the two types of calculations we performed to construct the entire complex potential surface for the $^2B_1$ state, turning first to the electron-molecule scattering calculations necessary for computing the width.

A. The complex Kohn variational method

The complex Kohn variational method makes use of a trial wave function that is expanded in terms of square-integrable (Cartesian Gaussian) and continuum basis functions that incorporate the correct asymptotic boundary conditions. Detailed descriptions of the method have been given elsewhere (see, for instance, refs. [15, 16]), so here we will limit ourselves to a very brief summary to establish the terminology we will use to describe our numerical calculations.

The physics of a calculation using the complex Kohn variational method is exhibited in the trial function, which, for a target containing N electrons, has the form

$$\begin{aligned}\Psi^{(+)}_{\Gamma_0} = &\sum_{\Gamma} \mathcal{A}\left[\chi_\Gamma(\mathbf{r}_1 ... \mathbf{r}_N) F^{(+)}_{\Gamma,\Gamma_0}(\mathbf{r}_{N+1})\right] \\ &+ \sum_{\mu} d^{\Gamma_0}_{\mu} \Theta_\mu(\mathbf{r}_1 ... \mathbf{r}_{N+1}) \quad .\end{aligned} \tag{2}$$

The first sum in Eq. (2) is over target states explicitly included in a close-coupling expansion, which may be energetically open or closed, and for which $\chi_\Gamma(\mathbf{r}_1 ... \mathbf{r}_N)$ denotes the corresponding electronic state of the target molecule. The antisymmetrizer is denoted by $\mathcal{A}$, and the scattering orbital (channel eigenfunction) associated with channel Γ is

$$\begin{aligned}F^{(+)}_{\Gamma,\Gamma_0}(\mathbf{r}) = &\sum_i c^{\Gamma,\Gamma_0}_i \varphi_i(\mathbf{r}) \\ &+ \sum_{l,m} \left[f_{l,m}(k_\Gamma r)\delta_{l,l_0}\delta_{m,m_0}\delta_{\Gamma,\Gamma_0}\right. \\ &\left. + T^{\Gamma,\Gamma_0}_{l,l_0,m,m_0} g^{(+)}_{l,m}(k_\Gamma r)\right] Y_{l,m}(\hat{\mathbf{r}})/r\end{aligned} \tag{3}$$

for incoming boundary conditions in channel Γ_0. In Eq. (3) φ_i denotes a Gaussian molecular orbital, and $f_{l,m}(k_\Gamma r)$ and $g^{(+)}_{l,m}(k_\Gamma r)$ denote continuum functions which are regular at the origin and whose asymptotic forms correspond to Ricatti-Bessel and outgoing Ricatti-Hankel functions, respectively:

$$f_{l,m}(k_\Gamma r) \underset{r\to\infty}{\longrightarrow} j_l(k_\Gamma r)/\sqrt{k_\Gamma} \tag{4}$$

$$g^{(+)}_{l,m}(k_\Gamma r) \underset{r\to\infty}{\longrightarrow} h^{(+)}_l(k_\Gamma r)/\sqrt{k_\Gamma} \quad . \tag{5}$$

With each of these continuum functions is associated a channel momentum, k_Γ

$$k^2_\Gamma/2 = E - E_\Gamma \quad . \tag{6}$$

The second sum in Eq.(2) is over square integrable (N+1)-electron terms (configuration state functions) constructed from Gaussian molecular orbitals and incorporates correlation effects not described by the close-coupling expansion of the first sum. For convenience we refer to the (N+1)-electron configurations, Θ_μ, in the second sum as the "Q-space" and to the square-integrable (N+1)-electron configurations involving target configurations and the orbitals φ_i generated by the antisymmetrizer in the first sum as the "P-space" of the calculation.

Inserting the trial wave function into the variational principle

$$T^{\Gamma,\Gamma_0}_s = T^{\Gamma,\Gamma_0}_t - 2\int \Psi^{(-)*}_\Gamma (H-E)\Psi^{(+)}_{\Gamma_0} d\mathbf{r}_1 ... d\mathbf{r}_{N+1} \tag{7}$$

yields a set of linear equations for the coefficients c_i^{Γ,Γ_0}, $d_\mu^{\Gamma_0}$, and the T-matrix, whose elements are denoted as $T_{l,l_0,m,m_0}^{\Gamma,\Gamma_0}$. The cross sections can be constructed from the T-matrix, and in the present case the width and position of the $^2B_1$ resonance are extracted from its eigenphases.

A description of a complex Kohn calculation therefore requires the specification of the approximate target states χ_Γ, the correlating configurations Θ_μ, and, for the expansion of the channel eigenfunctions, the Gaussian molecular orbitals φ_i and the l, m pairs included in the asymptotic partial wave expansion.

B. Target states and basis set of the complex Kohn variational calculations

The square integrable portion of the basis used to construct the Kohn trial function consisted of the Gaussian basis set of Gil *et al.* [10], augmented with additional diffuse orbitals. On the oxygen, we added an s function with exponent 0.0316 and a p function with exponent 0.0254; on each of the hydrogens, we added s functions with exponents 0.08 and 0.0333, and p functions with exponents 0.2 and 0.05. With these additions, our basis set included a total of 77 functions.

The orbital space spanned by this basis set was divided into sets of "target orbitals" and "scattering orbitals." The target orbitals were the set $\{1a_1, 2a_1, 1b_2, 3a_1, 1b_1, 4a_1, 2b_2, 5a_1\}$, which were obtained from natural orbital calculations on the ground state and on the resonance, as described below. The scattering orbitals were the orthogonal complement of the target orbitals.

At each geometry, the first five target orbitals were obtained from a multi-reference plus all single excitations configuration-interaction calculation on the neutral ground state. The orbital basis for these calculations consisted of the five occupied SCF orbitals along with a set of "improved virtual orbitals" calculated in the field of the (N-1)-electron Hamiltonian obtained by singly occupying the highest occupied molecular orbital. (This orbital was almost always the $1b_1$ / $1a''$ orbital.) We performed complete active space (CAS) CI calculations in this basis, doubly occupying the $1a_1$ orbital and distributing the eight remaining electrons over all possible configurations that could be generated from the set of actve orbitals $\{2a_1, 1b_2, 3a_1, 1b_1, 4a_1, 2b_2\}$. We also included all single excitations obtained by placing seven electrons in the active space and the remaining electron in an IVO orbital. This generated a CI expansion of ∼15,000 terms. The first five "target" orbitals used in the complex Kohn trial function were the natural orbitals obtained by diagonalizing the ground state density matrix from this CI calculation.

We then performed similar calculations for the anion state, beginning with a set of occupied orbitals from a symmetry-restricted SCF calculation on the $^2B_1$ resonance state. We carried out a CI calculation in $^2B_1$ symmetry, keeping the $1a_1^2 2a_1^2 1b_2^2 3a_1^2 1b_1^1$ occupancy of the five inner orbitals fixed, and allowing two electrons to occupy any of the remaining a_1 and/or b_2 orbitals. The $4a_1$, $2b_2$ and $5a_1$ orbitals were obtained by diagonalizing the density matrix of the lowest energy root. We found that we could improve this set of natural orbitals via an iterative scheme where each iteration consisted of a symmetry-restricted, multi-reference plus all singles CI calculation where the reference space was obtained by distributing eleven electrons over the $\{1a_1, 2a_1, 1b_2, 3a_1, 1b_1, 4a_1, 2b_2, 5a_1\}$ natural orbitals, with the constraint that the $1a_1$ and $1b_1$ orbitals be doubly and singly occupied, respectively, in each configuration. The size of the configuration space for these last calculations was ∼13000 in C_{2v} symmetry and ∼25000 in C_s symmetry. Four iterations were performed.

The final set of eight target orbitals used in the complex Kohn trial funnction consisted of the five natural orbitals with the highest occupation numbers – invariably, the orbitals $\{1a_1, 2a_1, 2b_2, 3a_1, 1b_1\}$ – from the neutral ground state calculations, combined with the $4a_1$, $2b_2$, and $5a_1$ natural orbitals from the anion calculations, the latter Schmidt orthogonalized to the former. The remaining unoccupied orbitals – the scattering orbitals, φ_i in Eq. (3) – were also taken from the anion calculations and Schmidt orthogonalized to the five natural orbitals from the ground state calculations.

Seven states χ_Γ were explicitly included in the P-space portion of the Kohn trial function in Eq.(2). These states were defined as the roots of a complete active space CI within the space of the target orbitals $\{2a_1, 1b_2, 3a_1, 1b_1, 4a_1, 2b_2, 5a_1\}$, with the $1a_1$ orbital always doubly occupied. For energetically closed channels, only L^2 functions φ_i were included in the expansion of $F_{\Gamma,\Gamma_0}^{(+)}$ in Eq.(3). At each nuclear geometry, the seven target states with the lowest energy were chosen. Near the equilibrium geometry, this included the $^1A_1$ ground state and the $^{1,3}B_1$, $^{1,3}A_2$, and $^{1,3}A_1$ excited states. The target energies at the equilibrium geometry of water are listed in Table I.

TABLE I: H_2O target energies at equilibrium geometry. Complex Kohn values are compared with results of van Harrevelt and van Hemert [24]. Energies from this work are calculated at $r_1 = r_2 = 1.81$ bohr, $\theta = 105°$. Energies from Ref. [24] were calculated at $r_1 = r_2 = 1.8$ bohr, $\theta = 104.5°$.

State	Energy (hartree)	Excitation Energy (electron volts)	
	complex Kohn	complex Kohn	Ref. [24]
$^1A_1$	-76.0581	0.0	0.0
$^3B_1$	-75.7795	7.582	
$^1B_1$	-75.7666	7.932	7.63
$^3A_2$	-75.7086	9.511	
$^1A_2$	-75.7049	9.611	9.60
$^3A_1$	-75.6933	9.926	
$^1A_1$	-75.6710	10.534	9.95

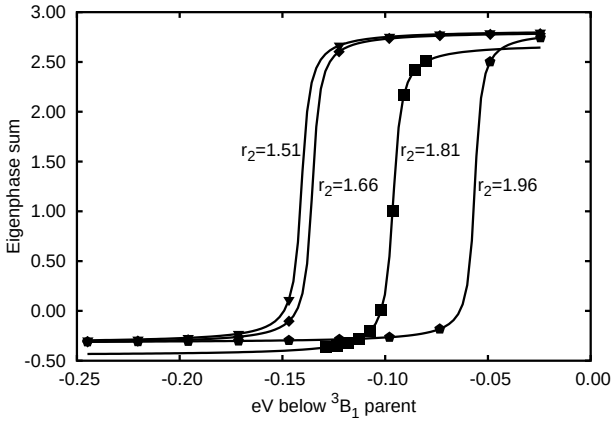

FIG. 2: Eigenphase sums, in radians. r_1 is fixed at 1.81, θ at 105°, and r_2 is varied. Distances in bohr.

The Q-space terms Θ_μ were comprised of all configurations that could be generated by placing eleven electrons within the space of target orbitals, subject to the constraint that the $1a_1$ orbital be doubly occupied. These so-called "penetration" terms contain the dominant configurations that describe the Feshbach resonances, as well as terms that relax any constraints imposed on the channel eigenfunctions that arise from the orthogonality among the scattering orbitals, continuum orbitals, and target orbitals [15].

The expansion of the continuum functions $F^{(+)}_{\Gamma,\Gamma_0}$ in Eq.(3) included $Y_{l,m}$'s spanning the range $l = 0$ to 4, with all values of m included for each target state consistent with overall $^2B_1$ or A″ symmetry.

C. Calculation of the resonance widths

The complex Kohn calculations were performed over a grid in valence coordinates on which the OH bond lengths took on values r ={1.51, 1.81, 2.11, 2.41, 2.71, 3.01, 3.61 bohr} and the angles were θ ={15, 30, 45, 60, 75, 90, 105, 120, 135, 150, 165°}. Geometries at θ ={15, 30} which are energetically inaccessible to the dissociative attachment process were not included.

To facilitate locating the resonance position at each geometry, we first diagonalized the energy-independent portion of the Kohn Hamiltonian, constructed from square-integrable basis functions, and inspected the low-lying eigenvalues and eigenvectors to locate the resonance root. The full scattering calculation was then performed at ten energies around the resonance location and the corresponding eigenphase sums were tabulated and fitted to a Briet-Wigner form with a linear background to extract the resonance positions and widths. Eigenphase sums for several representative geometries are shown in Fig. 2.

The complex Kohn calculations produce a narrow $^2B_1$ resonance that lies close to – and generally below – its $^3B_1$ parent state. At several geometries, however, the resonance pole appeared slightly ($\sim$ .1 eV) above its $^3B_1$ parent state. Unfortunately, we were unable to reliably perform the Kohn calculation at energies close enough to threshold to get meaningful Breit-Wigner fits in these cases. The imaginary part of our interpolated resonance surface was therefore constructed under the assumption that the $^2B_1$ resonance always lies below its parent. We will have more to say about this below.

D. CI calculation for real part of resonance surface

In the asymptotic regions where the anion is electronically bound, we can use electronic structure methods to compute the anion potential surface. As we stated earlier, the resonance widths are so narrow in this case that we can use these same techniques at all geometries of interest. This strategy allows us to use large-scale CI techniques to compute the real part of the resonance surface at all geometries. It also spares us the difficulties that would be encountered in trying to match the energy surface obtained from scattering cqalculations in one region with the asymptotic portions of the surface obtained by a different method.

The real part of the resonance surface was approximated by large-scale, multi-reference configuration-interaction calculations with single and double excitations. For these calculations, we used the augmented, correlation-consistent, polarized valence triple-zeta basis set developed by Dunning and coworkers [25]. Molecular orbitals were first obtained via a symmetry-restricted SCF calculation on the $^2B_1$ resonance. The CI reference space included the $1b_2$, $3a_1$, $1b_1$, $4a_1$, $5a_1$, and $2b_2$ orbitals in C_{2v} symmetries, which correspond to 3a′, 4a′, 1a″, 5a′, 6a′ and 7a′ orbitals in C_s symmetries. The 4 electrons occuping the $1a_1$ and $2a_1$ orbitals, which are comprised of mainly the oxygen 1s and 2s orbitals, were fixed with double occupation and not correlated in these calculations. The $1b_2$ and $3a_1$ orbitals describe the two OH bonds, while the $1b_1$ orbital is a non-bonding orbital that describes the oxygen lone pair. The $4a_1$ (5a′) orbital, which is the resonance orbital near equilibrium geometry, becomes the 1s orbital of the H^- anion in the $OH + H^-$ arrangement. Inclusion of the $2b_2$ and $5a_1$ orbitals is important for describing correlation effects in the resonant state and permits the proper dissociation of the molecule. Configurations corresponding to all possible distributions of 7 electrons in the CI reference space were included in the CI Hamiltonian along with all single and double excitations from that reference space. The total number of configurations in these calculations was ∼900,000.

For this calculation, we defined a full grid of r_1, r_2 = {1.45, 1.55, 1.65, 1.75, 1.85, 1.95, 2, 2.25, 2.5, 2.6, 2.8, 3.0, 3.2, 3.4, 3.6, 3.8, 4.0, 4.2, 4.4, 4.6, 4.8, 5.0, 5.2, 5.6, 5.8, 6.0, 6.5, 7.0, 8.0, 9.0, 10.0, 11.0, 12.0 bohr}, θ={1, 2, 3, 4, 5, 6, 7, 8, 9, 10, 11, 12, 14, 15, 16, 17, 18, 20, 22,

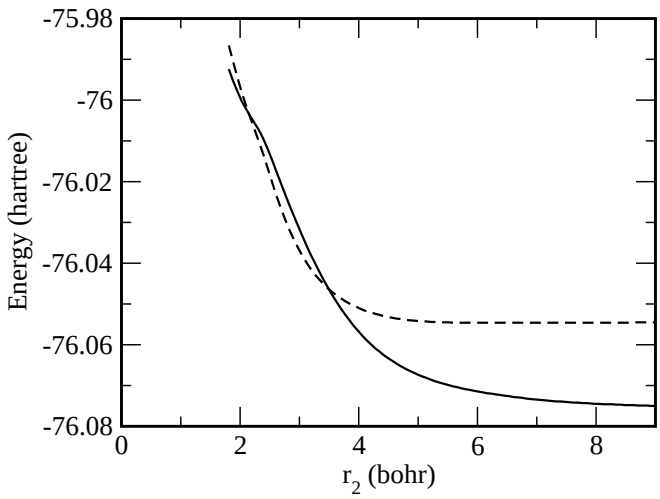

FIG. 3: $^2B_1$ resonance and $^3B_1$ neutral energies, from CI calculations, along the cut in valence-bond coordinates with $r_1 = 1.81$ and $\theta = 105^0$: resonance energy (solid curve), neutral energy (dashed curve).

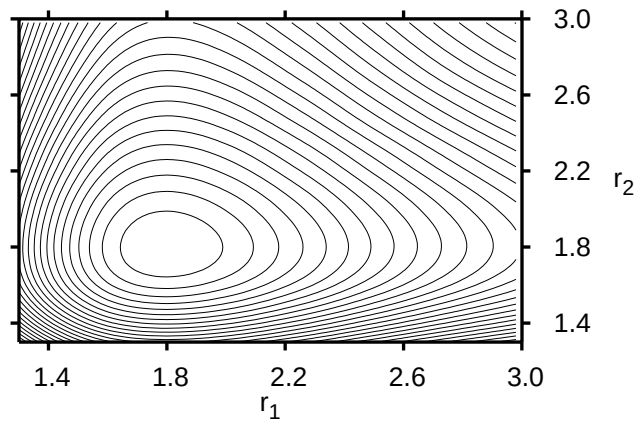

FIG. 4: Calculated ground state potential surface for $\theta = 104.5^0$ with contours every 0.25 eV. Bond lengths in bohr.

24, 25, 30, 35, 40, 45, 50, 55, 60, 65, 70, 75, 85, 100, 120, 140, 160, 175 degrees}. This $33 \times 33 \times 37$ grid includes 40293 points. But of these, on only 6025 appropriately chosen points were the CI calculations performed; as described below, the energies at the remainder were defined by interpolation among the calculated points. For none of the 6025 points did the resonance location exceed an absolute value of -75.8 hartree.

The CI calculations, just like the complex Kohn calculations, showed that for certain geometries the resonance state lies energetically slightly above its neutral parent. This is illustrated in Fig. 3. This was generally found to occur at geometries where one OH bond distance was close to its equilibrium value and the other was stretched by 1-2 bohr. These are geometries where H^- begins to overlap OH and it becomes difficult to maintain a consistent description of correlation in the neutral and anion states. It is also possible that we are looking at small basis set superposition errors at these geometries. In any case, we believe this is unlikely to be a physically correct result and therefore, as we observed above, the imaginary part of our interpolated resonance surface was constructed under the assumption that the $^2B_1$ resonance always lies below its parent. This issue will prove to be important in the discussion of experimentally observed isotope effects presented in the subsequent paper.

E. CI calculation for the ground state potential surface

For the calculation of the neutral potential surface, we followed a prescription similar to that used in generating the resonance surface. The number of orbitals used to define the active space was the same, with the difference that six, not seven, electrons occupy the reference space of $1b_2, 3a_1, 1b_1, 4a_1, 5a_1$ and $2b_2$ orbitals.

For the neutral, the full grid was specified by r_1, r_2 = {1.55, 1.6, 1.65, 1.7, 1.72, 1.74, 1.76, 1.78, 1.8098, 1.82, 1.84, 1.86, 1.88, 1.9, 1.92, 2, 2.25, 2.5, 2.75, 3.0 bohr}, and θ={20, 40, 60, 80, 100, 120, 140, 160, 175 degrees}. The CI calculation was performed on each point on this grid.

The neutral surface was represented by a three-dimensional cubic spline fit using the full grid of points obtained from the CI calculation described above. It is convenient to have a representation of the potential far into the classically forbidden region, and to that end the potential was extrapolated beyond the end of the computed grid using a quadratic representation. The ground state potential surface is shown in Fig.4. This potential surface yields energies for the first few bound rovibrational states in good agreement with the spectroscopically accurate surface of Polyansky *et al.* [26]

IV. FITTING THE RESONANCE POTENTIAL ENERGY SURFACE

A. Real part of the resonance energy

To construct a complete representation of the real part of the resonance surface, a reference potential was first subtracted from the computed points and the remainder was fit with three-dimensional cubic splines. The reference potential is a sum of two-body terms consisting of three Morse potentials in the r_{OH} and r_{HH} coordinates. The reference potential plus the splined residual comprises the global fit of the surface which coincides exactly with the calculated points.

The Morse potentials were optimized for the asymptotic regions, one for each atom-diatom arrangement.

Thus,

$$V(r_1, r_2, \theta) = V_S(r_1, r_2, \theta) + V_{OH}(r_1) + V_{OH}(r_2) + V_{HH}(r_{HH}) \quad (8)$$

in which V_S is the splined residual, and r_{HH} is a function of the other three coordinates. The OH Morse potential was obtained by fitting the 124 most exterior points, yielding the fitted function (in atomic units)

$$V_{OH}(r) = 0.1534(1 - \exp(1.344(1.809 - r)))^2 \quad (9)$$

with rms error 0.0032. The HH Morse potential was fit using 69 points at large $H_2 + O^-$ separations which simultaneously satisfied the conditions that $r_1, r_2 > 8$ and $r_{HH} < 4$, yielding

$$V_{HH}(r) = 0.1827(1 - \exp(1.098(1.406 - r)))^2 \quad (10)$$

with rms error 0.0029. These fits are certainly not spectroscopic – there are three-body interactions still present for many geometries at the exterior of our grid, and the fits above only represent the best two-body fits to the exterior regions of the full three-body potential.

The difference between the reference potential and the calculated values is therefore a combination of small corrections to the three two-body interaction potentials, plus the entire three-body interaction potential. This difference is the quantity which was fit with cubic splines to obtain $V_S(r_1, r_2, \theta)$ above.

The splining proceedure was performed in the valence-bond coordinate system using the calculated CI points. Since we did not calculate the full grid of points, a multi-step splining proceedure was required. First, a series of one-dimensional splines, in the θ direction and then along the r_1 and r_2 directions, was performed to obtain the surface at the remaining grid points. Second, the full grid of points thus constructed was fit to three-dimensional cubic splines.

Fig. 5 illustrates how the combination of an analytical reference potential and a splined residual produces a better representation of the full potential surface than what would be obtained with a direct three-dimensional spline fit of the calculated points. That advantage is particularly important in the $H_2 + O^-$ arrangement. The exiting well in this arrangement lies diagonally in the valence-bond coordinate system upon which our grid of calculated points is based. Our grid is also sparse in this asymptotic region. Thus, obtaining a reliable fit from a spline proceedure alone would be impossible. This is because the $H_2 + O^-$ potential energy surface – and in particular, the highly repulsive part at small H-H separations – is not easily described by the third-degree polynomials comprising the spline functions. To illustrate, consider the geometries (1) $\{r_1 = 7, r_2 = 7, \theta = 1°\}$ and (2) $\{r_1 = 7, r_2 = 8, \theta = 1°\}$, which are adjacent in our grid of points. Point (1) is high upon the repulsive wall of the H-H potential, whereas point (2) is closer to the H-H equilibrium separation. A pure spline would represent the behavior of the potential between these two points with a third-degree polynomial, which is a poor substitute for the behavior of the true potential (which is better approximated by an exponential or by $1/r^{12}$). The improvement gained by subtracting the analytic reference potential before fitting with splines is substantial, as shown in Fig. 5.

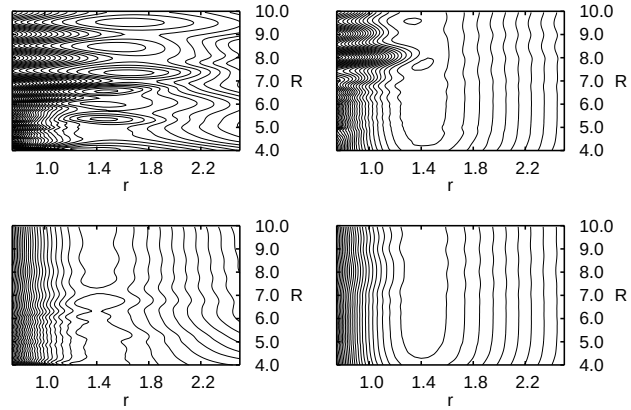

FIG. 5: H-H potential energy well in Jacobi ($r = r_{HH}$) coordinates, at $\gamma = 0$ (left) and $\gamma = 90°$ (right). The top panels represent a direct splined fit of the full surface; the bottom panels combine a reference two-body potential with a splined fit of the residual. Distances (r and R) in bohr; contours every 0.25eV.

Even with the improvement afforded by this technique, however, the $H_2 + O^-$ well is not represented with sufficient accuracy to afford reliable rotational or vibrational analyses for this rearrangement channel. Irregularities of approximately 0.25eV persist at linear O-H-H geometry. Fortunately, these irregularities are far removed from the $H^- + OH$ well and therefore do not affect dynamics leading to that arrangement.

B. The width of the resonance

The calculated values of the width were tabulated and the square root of the width was then fit in the valence-bond coordinate system to a basis set expansion of 60 symmetrized Gaussian functions of the form,

$$\phi_{ijk}(r_1, r_2, \theta) = (1 + P_{ij}) \left[(r_1/c_i)^2 + (r_2/c_j)^2\right]^{k/2} \exp\left[-(r_1/c_i)^2 - (r_2/c_j)^2\right] \cos(k\theta) \quad , \quad (11)$$

where P_{ij} is an operator which permutes indices i and j. The coefficients c_i are $\{1.2, 1.4, 1.6, 1.8, 2.0\}$ and the integer k runs from 0 to 3 inclusive. This basis set was used in a least-squares fit of the square root of the width using the method of singular value decomposition [27]. The rank of the singular value decomposition matrix was 25 and the root-mean-square error of the width function thereby constructed was 0.00075eV. In Fig.6 we show

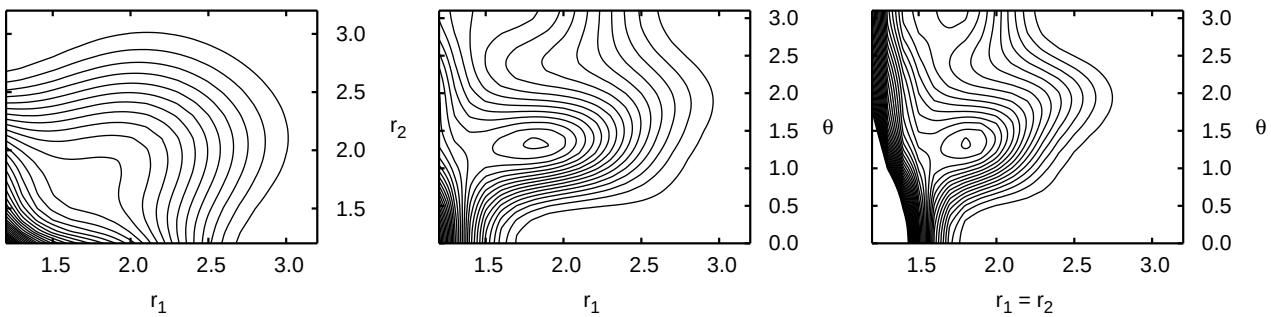

FIG. 6: Fitted width function in valence-bond coordinates at $\theta = 105$ degrees; $r_2 = 1.81$ bohr; and in C_{2v} geometry. θ in radians; r_1 and r_2 in bohr; contours every 0.0005eV.

three cuts of our fitted width function in valence bond coordinates.

The interested reader can access the data files and computer codes needed to generate the complex resonance energy at any desired geometry. These electronic files can be retrieved from the EPAPS archive [28].

C. Comparison with other calculations

Gorfinkiel, Morgan and Tennyson [12] have performed R-matrix calculations on one portion of this potential surface. They fixed one OH distance and the bond angle to be those of the ground state of water, and treated dissociation in one dimension along the other OH distance, r_2 in our notation. In Fig. 7 we compare our calculated widths and our fit of them with those of the R-matrix calculation. Our widths are uniformly larger than those of the R-matrix calculation. The behavior of the widths from our calculation is similar to that from the R-matrix calculation in that both show a maximum or a plateau around equilbrium ground-state neutral H_2O geometry, though the R-matrix values fall off somewhat more quickly with increasing r_2.

In Fig. 8 we compare the real part of the resonance potential energy surface calculated in the CI calculations described above with the R-matrix calculations of reference [12]. In this figure the resonance energies are shown relative to the energy of the ground state at equilibrium geometry in the corresponding calculation. Our CI calculations agree very well, both in shape and magnitude, with the R-matrix results for values of r_2 inward of the equilibrium value. For larger values of r_2 the CI potential surface is flatter in this cut than is the R-matrix surface.

Fig. 8 also shows the resonance energy from the complex Kohn calculations. In this one-dimensional cut of the full potential surface one can see that in the vicinity of the equilibrium geometry its shape is similar to that of the CI calculation, but its behavior for large r_2 differs. The large-scale CI calculations should be significantly more reliable in this limit because they have been designed to treat the dissociative limits correctly.

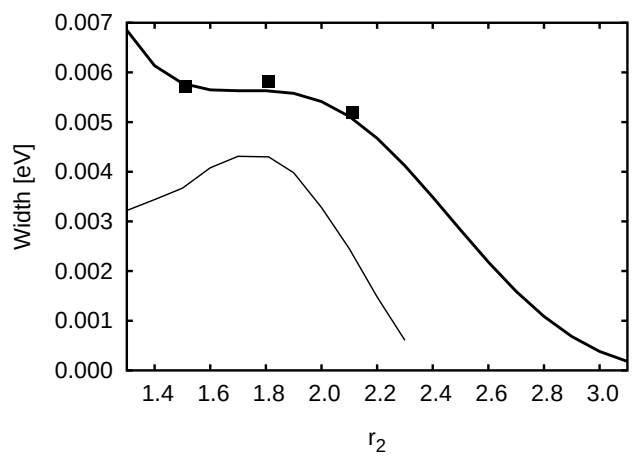

FIG. 7: Calculated width values (solid squares) and fitted width function (dark solid line) along the cut in valence-bond coordinates with $r_1 = 1.81$ bohr and $\theta = 105^0$ together with values from Gorfinkiel *et al.* [12] at $\theta = 104.5^0$ (light solid line). r_2 in bohr.

Fig. 9 compares the resonance energies from the complex Kohn and CI calculations at geometries where the OH bond distances are held fixed and the HOH bond angle is varied. Once again the shapes of the two curves are found to be very similar.

V. CHARACTERIZATION OF THE SURFACE

Several qualitative remarks about the expected shape of the $^2B_1$ resonance surface may be helpful before we describe the specific features of the potential energy surface we have constructed in these calculations.

First, the $^2B_1$ state is formed by the promotion of an electron from a nonbonding orbital to an antibonding orbital and the capture of a continuum electron into the same antibonding orbital. Thus, a superficial characterization of this state would indicate a bond order of 1,

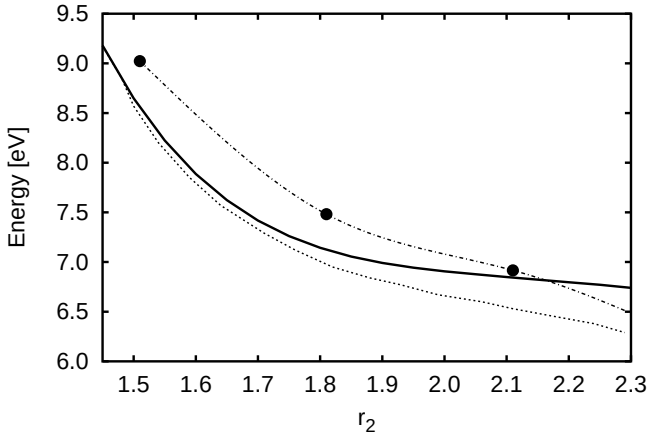

FIG. 8: Resonance energy along the cut in valence-bond coordinates with $r_1 = 1.81$ bohr and $\theta = 105^0$: complex Kohn calculations (solid dots connected by chained curve), present CI calculations (dark solid line) and calculations of Gorfinkiel *et al.* [12] at $\theta = 104.5^0$ (dotted line). r_2 in bohr.

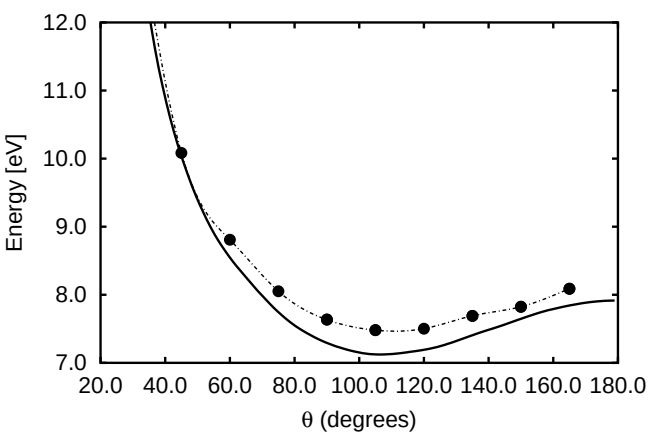

FIG. 9: Resonance energy as a function of θ with r_1 and r_2 fixed at 1.81 bohr: complex Kohn calculations (dots connected by chained curve), present CI calculations (solid line).

and therefore an overall dissociative shape of the potential energy surface near equilibrium ground-state H_2O geometry.

A second elementary expectation is that the anion surface should vary less with bending angle than does the ground state surface. The splitting of the energies of the $3a_1$ and $4a_1$ orbitals is enhanced by the $s-p$ hybridization afforded by bent geometries; that effect is one explanation of the origin of the molecule's bent equilibrium geometry, as H_2O in its ground state has two electrons in the $3a_1$ but none in the $4a_1$ orbital. In the $^2B_1$ state both $3a_1$ and $4a_1$ orbitals are doubly occupied. As the bending angle is increased from its equilibrium value, the increase in the $3a_1$ orbital energy is accompanied by a decrease in the $4a_1$ orbital energy and the $^2B_1$ state is thus expected to have a potential energy surface which is relatively flat with bending angle.

The entire potential surface is surveyed in Fig. 10 in valence bond coordinates. Cuts are given that vary in the bond angle, θ, from 0° to 180°. From these cuts we can see some of the expected features. $O^- + H_2$ is visible in the cut at $\theta = 0°$ as two narrow channels for which $|r_1 - r_2| = 1.4$ bohr. In the valence-bond coordinate system, this channel has the shape of a tube, a higher part of which can be seen in the next cut at $\theta = 15°$.

As the bond angle is increased we see more clearly the wells corresponding to the arrangement $OH + H^-$. As can be seen in the top panel of the right column of Fig. 10, at the equilibrium geometry of neutral H_2O the gradient of the surface is quite steep in the symmetric stretch direction. At $\theta = 104.5°$, the surface posesses a saddle point at $r_1 = r_2 \approx 2.1$, and then increases in energy as the symmetric stretch coordinate is further increased. On either side of this saddle, the $OH + H^-$ wells form quickly and the gradient in the r_1 or r_2 direction is large. Relative to its rapid variation in r_1 or r_2, the variation of the surface with respect to θ is generally small in the vicinity of the equilibrium geometry of the neutral.

Although it does not affect the dissociation dynamics because autodetachment is negligible immediately beyond the Franck-Condon region, it is nevertheless interesting to see where the resonance state becomes electronically bound, ie. where it crosses the ground-state surface of neutral water. To locate these crossings, which lie well outside the range of geometries where we needed to compute the neutral target surface, we used the spectroscopically accurate potential energy surface of water computed by Polyansky, Jensen and Tennyson [26], shifted to coincide with the minimum of our calculated CI surface. The points at which the resonance and neutral surfaces cross are plotted in Fig.10. Since the surface of Polyansky *et al.* is a spectroscopic fit and thus not expected to represent the dissociative limits correctly, the crossings depicted in Fig. 10 should be considered to be estimates, especially for cuts such as that at θ=105 degrees, in which the crossing occurs at relatively large bond lengths.

Although Fig. 10 in principle gives a complete view of the surface, some features are easier to see in other coordinate systems. For example, the $O^- + H_2$ channel is more easily seen in the triangular coordinates used in Fig. 11 and sketched in Fig. 1. There is a local C_{2v} minimum on the surface in linear geometry at $r_1 = r_2 \approx 2.4$, which can be found in the upper left part of Fig. 11 on the boundary line that denotes linear configurations. In a time-dependent view of the dissociative attachment dynamics, which we will use in the following paper, the initial wave packet starts out with $\langle r_{HH} \rangle = 2.91$ and $\langle r_{OH} \rangle = 1.83$. This geometry places it a significant distance away from the $H_2 + O^-$ well, as can be seen in

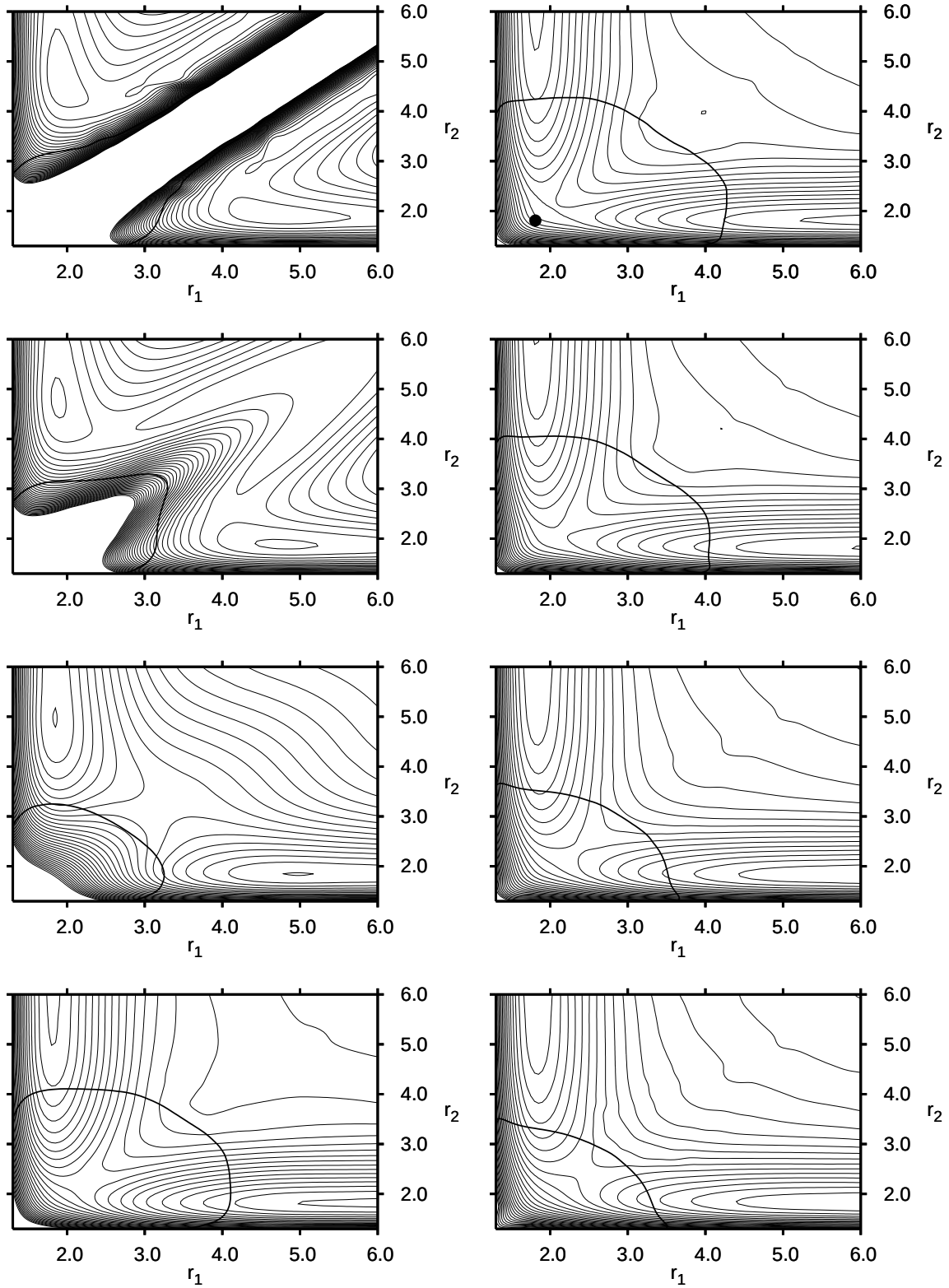

FIG. 10: Real part of the surface in valence-bond coordinates. Left column, top to bottom: $\theta = 0^0$, $\theta = 15^0$, $\theta = 35^0$, $\theta = 70^0$. Right column, top to bottom: $\theta = 104.5^0$, $\theta = 125^0$, $\theta = 150^0$, $\theta = 180^0$. Black dot for $\theta = 104.5^0$ denotes ground state equilibrium position. r_1 and r_2 in bohr; contours every 0.25eV. Thick curve on each panel denotes geometries where the resonance state crosses the neutral ground state (see text).

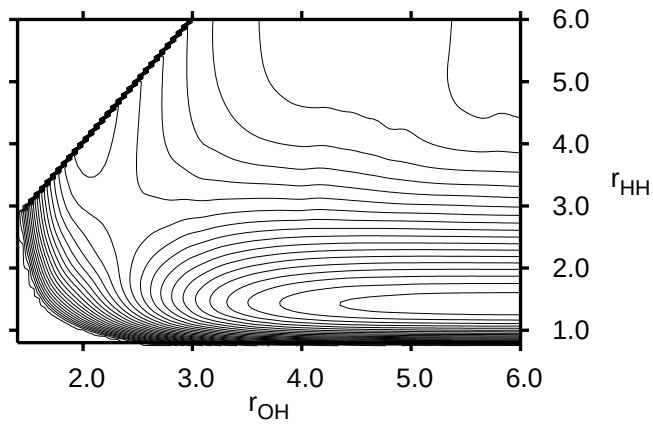

FIG. 11: Real part of the surface in C_{2v} symmetry in triangular coordinates. Distances in bohr; contours every 0.25eV.

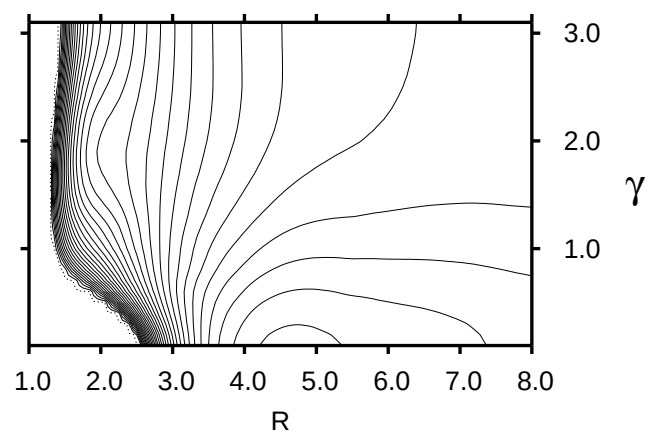

FIG. 12: Real part of the surface in Jacobi ($r = r_{OH}$) coordinates at $r = 1.81$. R in bohr; γ in radians; contours every 0.25eV.

Fig. 11 . In the cut in this figure, the $H_2 + O^-$ well appears dissociative throughout. However, as C_{2v} geometry is broken, there develops a very weak, broad global minimum of the surface in the $H_2 + O^-$ well at $r_1 \approx 5.5$, $r_2 \approx 4$, $\theta = 0°$. This well can be interpreted as a polarizable H_2 bound to the O^-.

The Feshbach resonances relevant to dissociative attachment in water can be characterized as an extra electron weakly bound to the corresponding parent states. Thus, at least in the region where this state is a resonance, we expect the shape of the $^2B_1$ potential energy surface to closely parallel that of its parent $^3B_1$ state. In the asymptotic region, where the resonance becomes bound, the electronic energy of the resonance drops significantly below that of its parent as the electron affinity of the fragments is recovered.

The potential surface of the $^3B_1$ neutral state is itself similar to that of the $^1B_1$ state. The latter is responsible for the photodissociation of water in its first absorption band, which has been called "the most studied triatomic photochemical reaction" [29]. Numerous calculations have been performed on this state, and it is illuminating to compare its potential surface with the present resonance surface.

For instance, van Harrevelt and van Hemert [24] have constructed and used a potential energy surface for the $^1B_1$ state. They find a minimum in the symmetric stretch direction near $r_1 = r_2 = 2.05$ bohr for $\theta = 105°$. In the r_1 or r_2 directions, their potential is steeply dissociative at neutral H_2O equilibrium geometry, flattening out by approximtely $r_1 = 5$ bohr. Their surface is reasonably flat in θ, although they find a minimum in the $^1B_1$ potential near $\theta = 105°$ for $r_1 = r_2 = 1.8$ bohr, which is approximately 0.8eV lower than the energy at linear H-O-H geometry at those bond lengths.

Some parallels with the $^1B_1$ state can be seen in the cut of the $^2B_1$ surface shown in Fig. 12. We can see that the surface is relatively flat in the Jacobi angle, γ, though it favors a bent geometry at small bond lengths and a linear geometry at larger bond lengths. Interestingly, at $r_1 = r_2 = 1.8$ bohr, the difference between the minimum in energy at 105° and the energy at linear H-O-H geometry is 0.807eV, very similar to that calculated for the $^1B_1$ state of neutral water in ref. [24].

The relative accessibility of the $H_2 + O^-$ and $OH + H^-$ wells from equilibrium H_2O geometry is relevant to the branching ratios for this dissociative attachment process. While the $H_2 + O^-$ exit well includes the lowest points on the potential energy surface, it is not as immediately accessible from ground-state equilibrium geometry as is the $OH + H^-$ well. The steepest descent path of the potential energy surface does in fact lead from equilibrium geometry into the $O^- + H_2$ well, but it does so only by first stretching one OH bond from equilibrium geometry to approximately $r = 4$, and then tracing a wide arc to $\gamma = 0$ across a relatively flat region of the potential energy surface, near the cut shown in Jacobi coordinates in Fig. 12. The most direct route to this well proceeds without breaking C_{2v} symmetry along the cut in Fig. 11, but in doing so moves almost perpendicular to the steepest descent path. In our dynamical studies we will see that a wave packet originally located at the equilibrium geometry has a strong tendency to bifurcate into the steeply dissociative $H^- + OH$ wells. Thus it is the shape of the potential surface and not the overall energetics that controls the branching ratio into the two possible arrangement channels for dissociative attachment through this resonance.

VI. CONCLUSION

We have calculated the potential energy surfaces necessary for a description of dissociative eletron attachment to H_2O. In an accompanying article we examine the nuclear dynamics on this surface in an effort to obtain the dissociative attachment cross section.

Acknowledgments

This work was performed under the auspices of the US Department of Energy by the University of California Lawrence Berkeley National Laboratory under Contract DE-AC03-76SF00098 and was supported by the U.S. DOE Office of Basic Energy Sciences, Division of Chemical Sciences.

[1] W. N. Lozier, Phys. Rev. **36**, 1417 (1930).
[2] C. E. Melton, J. Chem. Phys. **57**, 4218 (1972).
[3] I. S. Buchel'nikova, Zh. Eksperim. i Teor. Fiz. **35**, 1119 (1959).
[4] G. J. Schultz, J. Chem. Phys. **44**, 3856 (1966).
[5] R. N. Compton and L. G. Christophorou, Phys. Rev. **154**, 110 (1967).
[6] S. Trajmar and R. I. Hall, J. Phys. B: At. Mol. Phys. **7**, L458 (1974).
[7] D. S. Belic, M. Landau, and R. I. Hall, J. Phys. B: At. Mol. Phys. **14**, 175 (1981).
[8] C. R. Claydon, G. A. Segal, and H. S. Taylor, J. Chem. Phys **54**, 3799 (1971).
[9] M. Jungen, J. Vogt, and V. Staemmler, Chem. Phys. **37**, 49 (1979).
[10] T. J. Gil, T. N. Rescigno, C. W. McCurdy, and B. H. L. III, Phys. Rev. A **49**, 2642 (1994).
[11] L. A. Morgan, J. Phys. B: At. Mol. Opt. Phys. **31**, 5003 (1998).
[12] J. D. Gorfinkel, L. A. Morgan, and J. Tennyson, J. Phys. B **35**, 543 (2002).
[13] S. Goursaud, M. Sizun, and F. Fiquet-Fayard, J. Chem. Phys **65**, 5453 (1976).
[14] S. Goursaud, M. Sizun, and F. Fiquet-Fayard, J. Chem. Phys **68**, 4310 (1978).
[15] T. N. Rescigno, B. H. L. III, and C. W. McCurdy, in *Modern Electronic Structure Theory*, edited by D. R. Yarkony (World Scientific, Singapore, 1995), vol. 1, pp. 501–588.
[16] T. N. Rescigno, C. W. McCurdy, A. E. Orel, and B. H. L. III, in *Computational Methods for Electron-Molecule Collisions*, edited by W. M. Huo and F. A. Gianturco (Plenum, New York, 1995).
[17] T. F. O'Malley and H. S. Taylor, Phys. Rev. **176**, 207 (1968).
[18] T. F. O'Malley, Phys. Rev. **150**, 14 (1966).
[19] Bardsley and Wadehra, J. Chem. Phys. **78**, 7227 (1983).
[20] M. Beck, A. Jackle, G. Worth, and H.-D. Meyer, Physics Reports **324**, 1 (2000).
[21] G. A. Worth, M. H. Beck, A. Jäckle, and H.-D. Meyer, The MCTDH Package, Version 8.2, (2000). See http://www.pci.uni-heidelberg.de/tc/usr/mctdh/.
[22] A. Jackle and H.-D. Meyer, J. Chem. Phys. **105**, 6778 (1996).
[23] C. E. Klots and R. N. Compton, J. Chem. Phys. **69**, 1644 (1978).
[24] R. van Harrevelt and M. C. van Hemert, J. Chem. Phys. **112**, 5777 (2000).
[25] R. A. Kendall, J. T. H. Dunning, and R. J. Harrison, J. Chem. Phys. **96**, 6796 (1992).
[26] O. L. Polyansky, P. Jensen, and J. Tennyson, J. Chem. Phys. **105**, 6490 (1996).
[27] J. W. Demmel, *Applied Numerical Linear Algebra* (SIAM, Philadelphia, 1997).
[28] See EPAPS Document No. E-PLRAAN-XX-XXXXXX for codes and data files needed to compute the complex potential surface at arbitrary geometries. A direct link to this document may be found in the online article's HTML reference section. This document may also be reached via the EPAPS homepage (http://www.aip.org/pubservs/epaps.html) or from ftp.aip.org in the directory /epaps/. See the EPAPS homepage for more information.
[29] R. van Harrevelt and M. C. van Hemert, J. Chem. Phys. **114**, 9453 (2001).